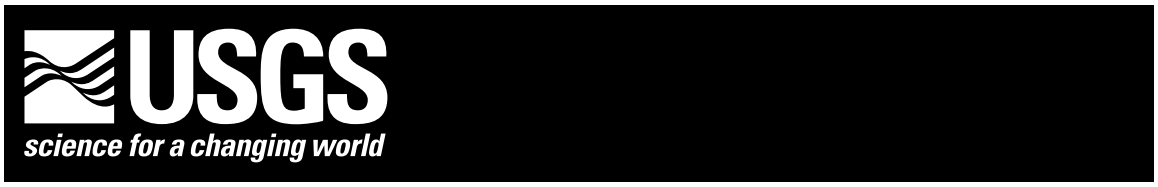

Timing of Paleoearthquakes on the Northern Hayward Fault — Preliminary Evidence in El Cerrito, California

By the **Hayward fault Paleoearthquake Group (HPEG)**[1]

Open-File Report 99-318

1999

U. S. DEPARTMENT OF THE INTERIOR
U. S. GEOLOGICAL SURVEY

[1]J. J. Lienkaemper & D.P. Schwartz, USGS 977, 345 Middlefield Rd., Menlo Park, CA 94025;
K.I. Kelson, W.R. Lettis, G.D. Simpson &, Wm. Lettis Assocs., 1777 Botelho Ave., Ste 262, Walnut Creek, CA 94596;
J.R. Southon, Center for AMS, L-397, Lawrence Livermore National Lab, 7000 East Ave., Livermore, CA 94551-9900;
J.A. Wanket, Dept. of Geography, 501 McCone Hall, UC Berkeley, Berkeley, CA 94720
P.L. Williams, Seismographic Station, 475 McCone Hall, UC Berkeley, Berkeley, CA 94720

Abstract

The Working Group on California Earthquake Probabilities estimated that the northern Hayward fault had the highest probability (0.28) of producing a M7 Bay Area earthquake in 30 years (*WGCEP*, 1990). This probability was based, in part, on the assumption that the last large earthquake occurred on this segment in 1836. However, a recent study of historical documents concludes that the 1836 earthquake did not occur on the northern Hayward fault, thereby extending the elapsed time to at least 220 yr ago, the beginning of the written record. The average recurrence interval for a M7 on the northern Hayward is unknown. *WGCEP* (1990) assumed an interval of 167 years. The 1996 Working Group on Northern California Earthquake Potential estimated ~210 yr, based on extrapolations from southern Hayward paleoseismological studies and a revised estimate of 1868 slip on the southern Hayward fault.

To help constrain the timing of paleoearthquakes on the northern Hayward fault for the 1999 Bay Area probability update, we excavated two trenches that cross the fault and a sag pond on the Mira Vista golf course. As the site is on the second fairway, we were limited to less than ten days to document these trenches. Analysis was aided by rapid C-14 dating of more than 90 samples which gave near real-time results with the trenches still open. A combination of upward fault terminations, disrupted strata, and discordant angular relations indicates at least four, and possibly seven or more, surface faulting earthquakes occurred during a 1630-2130 yr interval. Hence, average recurrence time could be <270 yr, but is no more than 710 yr. The most recent earthquake (MRE) occurred after AD 1640. Preliminary analysis of calibrated dates supports the assumption that no large historical (post-1776) earthquakes have ruptured the surface here, but the youngest dates need more corroboration. Analyses of pollen for presence of non-native species help to constrain the time of the MRE. The earthquake recurrence estimates described in this report are preliminary and should not be used as a basis for hazard estimates. Additional trenching is planned for this location to answer questions raised during the initial phase of trenching.

Introduction

The northern Hayward fault extends for ~50 km, from San Leandro to beneath San Pablo Bay, next to the most densely populated parts of the East [San Francisco] Bay Area. The *Working Group on California Earthquake Probabilities* (1990; WGCEP90) assigned a reliability ranking to the 30-yr probability of occurrence of major earthquakes on each of six selected fault segments in the Bay Area. They gave the northern Hayward (Fig. 1) and Rodgers Creek faults the lowest reliability rankings in the region, principally because these segments lacked reliable data for the most recent event (MRE). The MRE for the northern Hayward fault had been assumed to be a large earthquake in 1836 based on an unconfirmed historical interpretation by *Louderback* (1947). However, a recent detailed study of historical documents indicates this event occurred south of the Bay Area (Toppozada and Borchardt, 1998). Thus, the MRE for the northern Hayward fault is pre-1776, the date suggested by *Toppozada and Borchardt* (1998) for the start of the regional historical record. Because knowing the age of the MRE is essential for the calculation of time-dependent earthquake probability, constraining the maximum age bound of the MRE is critical information for forecasting major earthquakes on the Hayward fault. Another key objective of this research is the development of a late-Holocene paleoearthquake chronology for the northern Hayward fault. This would better constrain both the mean recurrence interval and the extent of ruptures, essential parameters for increasing the understanding of how the fault behaves and computing probabilities of future large earthquakes.

Constraining the northern extent of earthquake ruptures on the southern Hayward fault, including the M7 historical event in 1868, is required for evaluating fault segmentation and establishing a more realistic probability model. The WGCEP90 assumed that the 1868 rupture extended 36 km, from Agua Caliente Creek to Mills College (AC to MC, Fig. 1), based on information gathered 40 years after the earthquake (*Lawson,* 1908). A paleoearthquake study in Oakland (*Lienkaemper and others,* 1995; *Lienkaemper and Williams,* in press 1999) showed that surface rupture in 1868 extended at least as far north as Montclair Park (MT, Fig.1), and a new analysis of 19th century triangulation data suggested large slip at depth in 1868 as far north as Rocky Mound (RM, Fig.1; *Yu and Segall*, 1996). An estimated total length of 61 km or more for the 1868 subsurface rupture now seems reasonable (CR to RM, Fig. 1). Thus, confirming or excluding the occurrence of 1868 surface rupture at various locations along the northern Hayward fault is another important objective of our investigations.

This open-file report summarizes the results of the first phase of a paleoseismic trenching study across the Hayward fault at the Mira Vista golf course in El Cerrito, California. We present an overview of site selection, the methodology used, general stratigraphic relationships observed, and the evidence for paleoearthquakes. We then discuss the implications of these results with respect to the MRE, mean recurrence interval, and other potentially useful constraints on the timing of historical and prehistoric earthquakes at this site.

Trenching Results

Site selection

For site selection, we made a reconnaissance of the entire northern Hayward fault zone using aerial photography and made field inspections of the most promising sites. We concentrated our initial efforts north of Oakland to reduce possible complications from the overlapping of northern and southern segment ruptures. Shallow hand coring was done at 3 locations to help choose a site having optimal sedimentary layering and to determine the fault's exact location. The Mira Vista Golf Course site (Figs. 1, 2 and 3) was selected as the most favorable for having fine-scale stratigraphy across the active fault trace.

The favorable depositional environment at Mira Vista is due to a local anomaly in fault strike with respect to regional tectonics. A closed depression or sag pond has formed adjacent to the fault, presumably because the fault strikes N27°W locally. This strike is 8° more northerly than the N35°W average strike for the Hayward fault as a whole (*Lienkaemper*, 1992). This change in strike makes the fault more likely to have a sizeable extensional and vertical component of slip at this site. The Hayward fault generally seems to be well-oriented to release plate boundary motion as mainly strike-slip. Using regional strain data, *Lisowski and others* (1991) determined that the maximum right-lateral shear direction was N31.0°W ± 1.6° for the north Bay Area and N34.4°W ± 1.5° for the south and central Bay Area. This result is corroborated by more recent VLBI results (Sierra Nevada block-Pacific plate rotatation model, D. Argus, written commun., 1995) that give a net vector of N31°W at the midpoint of the Hayward fault. These values are all similar to the N33°W vector computed using the Nuvel-1A, Pacific- North America plate motion model, which spans the last 3.5 million years (*DeMets and others*, 1994). Thus, the tectonic setting of the site is well-suited to producing persistent vertical and extensional components of slip, that would contribute both to high rates of deposition and to a normal-oblique slip style of faulting, both of which greatly improve our ability to recognize paleoearthquakes in trench *exposures (Bonilla and Lienkaemper*, 1990).

Methodology

Because we were limited to only 10 days total for trench excavation, cleaning, logging, sampling, backfilling, and for repair of the golf-course, we assembled a team of 6 geologists. Many other personnel assisted in radiocarbon sampling, surveying, and photographing the walls. We cut two trenches to maximize exposure of paleoearthquake evidence; making trench 1 longer to expose a larger sample of the pond stratigraphy and explore for secondary faulting (location: Fig. 2, Fig. 3; logs: Fig. 4, Fig. 5). Trenching was done in mid-July to lessen ground-water problems. Although a permanent drain field had been installed, ground water is always within 1-2 m of the surface, so frequent pumping was needed.

We sampled for radiocarbon dating in three stages to achieve the fastest possible laboratory dating while the logging progressed. Samples taken in the first two days covered a wide range of stratigraphic horizons and were processed in 2-3 days by Lawrence Livermore National Laboratory's Center for Accelerator Mass Spectrometry (LLNL-CAMS). This allowed us to focus later stages of sampling on horizons most critical to dating the MRE and on other horizons important to establishing a complete paleoearthquake chronology for the past ~2,000 years. Altogether, about 90 radiocarbon samples were dated, predominantly on detrital charcoal (Table A1).

Stratigraphy

Although bedrock units adjacent to the fault are mapped in general as serpentinite southwest of the fault and as melange of the Franciscan Assemblage to the northeast (*Radbruch and Case*, 1967; *Dibblee*, 1980; *Graymer and others*, 1995), in our trenching, we found serpentinite on both sides of the main fault trace (Fig. 4). Southwest of the fault, the serpentinite is weathered to clay and rock fragments and is overlain by colluvial units of similar composition; below the northeasternmost pond sediments, the *in situ* serpentinite is highly-weathered but retains some rock structure.

Sag pond deposits have accumulated for at least the last 6,000 years at the site at an average rate of ~0.3 mm/yr. Deposition rates vary laterally and tend to be greater near the fault, up to 0.46 mm/yr. The pond sediments are composed of organic-rich silts and clays that are generally massive, but fine laminar structure is fairly abundant and variations in color made it possible to map and correlate several strata between trench exposures (Fig. 5). Drying of the pond deposits was essential to our recognition of sedimentary structure. Where walls remained saturated in the lower part of the trenches, little structure was observed.

The most distinctive units are four wildfire ash layers (units: u8, u15, u18, u24) that became the essential control strata for checking the overall correlation of the sequence. Adjacent to the main fault, a series of colluvial packages interfinger with the pond deposits and are derived principally from the intensely weathered serpentinite bedrock. Several minor unconformities exist near the fault, but the stratigraphic record as a whole appears complete and reliably dated for the ~2,200 years preceding the historic period. Units older than ~2,200 yr were saturated from the high water table, and few units were logged in detail or could be correlated reliably between the trenches.

A major erosional unconformity exists between units u27 and u28. A clean gray silty clay (u28) directly overlies the unconformity, and it is overlain by its more clast-rich equivalent (u29). These units are generally thicker, more massive and less organic-rich than the underlying pond deposits. Although we suspected that they were of historical age, we found no historical artifacts in them. However, pollen analysis of the pond sequence, shows that these gray units (u28, u29) both contain Eucalyptus, a tree that became widespread in the region during the 1880s. The next overlying unit (u30) is rockier than the underlying units,

and probably is a fill applied as an improvement to the golf course which was built circa World War I.

Paleoearthquakes

Paleoearthquakes are preserved in the stratigraphic record as relative changes in the amount of deformation between two adjacent units (called event horizons). Younger units are deformed less than older underlying units. Examples of features we interpret as evidence of past surface-rupturing earthquakes include: upward terminations of fault traces, disrupted strata, and discordant angular relations and scarp-derived colluvia. However, the occurrence of surface creep along the fault increases the difficulty in defining event horizons associated with coseismic surface rupture from paleoearthquakes. Because creep occurs on the Hayward fault (*Lienkaemper and others,* 1991; *Lienkaemper and Galehouse*, 1997), it is important to show that these increases in deformation downward derive from sudden, brittle surface-rupturing processes that we associate with large earthquakes, and not from gradual fault creep. We found evidence for nine possible deformation events in the sag pond deposits that we presently interpret as evidence of coseismic surface rupture. However, the ages of the three early events E1, E2, E3 are poorly constrained and resolution of stratigraphic and faulting features was much poorer in the lower, water-saturated stratigraphy, so we do not include these events in our discussion of recurrence interval. The stratigraphic sequence is reasonably well-dated for up to seven apparent ground-rupturing earthquakes, which we call E4, E5, E6, E8, E9, E10 and E11. In Figure 6 and Table 1, we summarize various evidence for each of these seven events in terms of its relative degree of certainty. Events E4, E6, E8 and E11 have clear evidence in most exposures. Events E3, E9 and E10 require the aggregation of more subtle evidence to suggest that they are distinct surface-rupturing events. Evidence for event E5 is fairly strong, but is less widespread among the exposures. One event that was initially interpreted, E7, was eliminated as our work correlating stratigraphic units progressed. Thus, there seem to be seven surface rupture events since 392 BC to 54 BC, four of which are more distinct (Tables 1 and 2), however this record could be incomplete for two reasons. Firstly, when such pond deposits are submerged, surface rupturing may occur with little or no brittle deformation and thus earthquake ruptures could either go undetected, or evidence for them might appear less distinct than for those occurring during the dry season. Secondly and perhaps even more important, an incomplete record of events can result simply from hiatuses in deposition. Further trenching is the best means of corroborating this preliminary event chronology and testing it for completeness.

Most Recent Event (MRE)

Because of the critical importance of the MRE to estimating the probability of future earthquakes, considerable attention was given to documenting the character of faulting and age constraints on event **E11**, which we judge to be the most recent event. We summarize evidence for the event **E11** in Table 1 and age constraints on it, in Figure 6 and Table 2. Some of the most conspicuous evidence for brittle fault slip in this event (on fault F2 above the u24/u25 contact, Fig. 5d) coincides with the best age control on the event (on unit u25). A weighted average of 4 radiocarbon dates from u25 gives calibrated age ranges of AD 1640 to 1679 (61% probability) and AD 1768 to 1802 (34%), thus constraining at >95% confidence the lower bound of the MRE (**E11**) to after AD 1640.

The upper-bound age for this event from radiocarbon data depends mostly on one sample (1S-21) from colluvium (u26). It is weakly corroborated by another sample (2N-10) with an identical radiocarbon date in a coeval silt unit (u27). However, this sample is from a krotovina, or infilled burrow and thus may be younger than the colluvium that surrounds it.

Age estimates from these samples suggest the minimum age constraint for the MRE (**E11**) is: 1) probably before 1821 (>88% confidence), 2) unlikely to be in 1868 (≤7% chance for 1837-1876), and 3) highly unlikely to be in 1836 (<<1%) (Table 2).

Equivocal or possible minor offsets on the major unconformity below the gray clay units (u28, u29), primarily in the south wall of trench 2, suggest the possibility that another event may have occurred after event **E11**. However, we believe that these features, such as an apparent fissure fill above fault F4 and soil steps in the u27/u28 contact, are better explained as resulting from erosion or fault creep. The soil steps on the u27/u28 contact in trench 2 (south wall) were logged schematically as abrupt steps but did not distinctly appear to be fault offsets. This interpretation is strongly supported by laboratory work that shows Eucalyptus pollen in the gray unit. Eucalyptus was not planted in the East Bay until the 1870s, and was not planted widely until the 1880s (see appendix for details on pollen analysis and history). Thus, displacements, if any, on the u27/u28 contact result from slip that has occurred after the 1868 earthquake, thus would almost certainly be due to aseismic slip.

The results of our study supports the hypothesis of *Toppozada and Borchardt* (1998), who conclude that the 1836 earthquake did not occur on the Hayward fault. Rather, a careful interpretation of the historical records of that period, suggests that there have been no large earthquakes on the Hayward fault since at least 1776. Based on the results presented here, we concur that 1776 is the best available estimate of minimum age for the MRE on the northern Hayward fault.

Recurrence interval

We consider age control reliable only for the past 7 events (E4 through E11). Event E7 was dismissed by improved stratigraphic correlation. To compute a minimum value for the mean recurrence interval, we use the minimum elapsed time for these seven or more events, 1627 years, which is derived from the 95% age bounds, AD 13 to 1640. This time period, 1627 yr divided by six intervals yields a minimum of <270 yr. Applying the less than symbol (<) to the minimum recurrence reiterates our concern that events might be missing from our record. At the other extreme, the four events with the most robust evidence (E4, E6, E8, E11) occurred after 355 BC and before AD 1776, i.e., three intervals in 2131 yr, or a maximum of 710 years.

We emphasize that this investigation is still in progress, and that we need to corroborate the paleoearthquakes thus far documented by logging other exposures and trenching other sites. Especially important, we need to confirm the completeness of the event record, because it is possible that some large earthquakes left no clear rupture evidence in the exposures logged to date.

Conclusions

The most recent event (MRE) is well-constrained by radiocarbon dating to have occurred after 1640. A single radiocarbon date supports the historical study of *Toppozada and Borchardt* (1998), which indicates that the 1836 earthquake was not on the northern Hayward fault and implies that the MRE was prehistoric or pre-1776. We observed no evidence that surface rupture occurred here associated with the 1868 earthquake, although some of the depositional record of this period is absent. A minimum of <270 yr for the mean recurrence interval is indicated by our preliminary interpretation of 7 surface-rupturing events, and allows that events could be missing. Using only the evidence for the 4 most-conspicuous paleoearthquakes gives a maximum mean recurrence time of <710 yr. More trenching is needed to verify the number and timing of paleoearthquakes on the northern Hayward fault. Existing radiocarbon constraints are not precise enough to indicate possible

clustering of events or to allow us to evaluate the variability in recurrence time. Recurrence intervals from this first phase of this paleoseismic investigation should not be used as a basis for computing hazard for the northern Hayward fault.

Acknowledgments

The National Earthquake Hazards Program of the U.S.G.S. funded both U.S.G.S. and William Lettis & Associates. Pacific Gas & Electric Company supported this work, especially in the reconnaissance phase, through its CRADA with the U.S.G.S. We thank so many for their timely assistance: especially Tom Fumal, John Hamilton, Daniella Pantosti, Chris Hitchcock, and many other staff and volunteers who lent a hand when it was most needed. We gratefully acknowledge the essential support and encouragement of the Directors, members and staff of the Mira Vista. Detailed and constructive reviews by Suzanne Hecker and Tom Fumal greatly improved the clarity of this report.

References

Bonilla, M. G. and Lienkaemper, J. J., Visibility of fault strands in exploratory trenches and timing of rupture events, *Geology 18*, 153-156, 1990.

Byrne, R., S. Mensing, and E. Edlund, Long term changes in the structure and extent of California Oaks, Final Report submitted to the Integrated Hardwood Range Management Program, 128 pp., 1993.

DeMets, C., R.G., Gordon, D.F. Argus, and S. Stein, Effects of recent revisions to the geomagnetic reversal of time scale on estimates of current plate motions, *Geophys. Res. Letts. 21,* 2191-2194, 1994.

Dibblee, T. W., Jr.. Preliminary geologic map of the Richmond quadrangle, Alameda and Contra Costa Counties, California, *U.S. Geol. Surv., Open-File Rep.* 80-1100, 1980.

Faegri, K., and J. Iversen, Textbook of Pollen analysis, New York, Wiley, 328 pp., 1989.

Frankel, R. E., Ruderal vegetation along some California Roadsides, Berkeley, University of California Press, 120 pp., 1967.

Gibbons, W.P., The redwood in the Oakland Hills, *Erythea 1*, 161-166, , 1893.

Graymer, R. W., D. L. Jones, and E.E. Brabb, Geologic map of the Hayward fault zone, *U.S. Geol. Surv., Open-File Rep.* 95-597, 1995.

Hayward Fault Paleoearthquake Group, The northern Hayward fault, CA: preliminary timing of paleoearthquakes, *EOS, Trans. Am. Geophys. Union 78,* 439, 1997.

Hendrey, G. W., Adobe brick as a historical source, *Agricultural History 8* , 64-71, 1931.

Lanson, J. A., Eucalyptus in California: its distribution, history, and economic value, MA Thesis, University of California, Berkeley, 210 pp., 1952.

Lawson, A. C., The earthquake of 1868 in A. C. Lawson, ed., The California earthquake of April 18, 1906, *Report of the State Earthquake Investigation Commission* (Volume I), Carnegie Institution of Washington Publication No. 87, 434-448, 1908.

Lienkaemper, J. J., Map of recently active traces of the Hayward fault, Alameda and Contra Costa Counties, California, *U.S. Geological Survey Miscellaneous Field Studies Map MF-2196*, map scale 1:24,000, 13 p., 1992.

Lienkaemper, J. J., and G. Borchardt, Holocene slip rate of the Hayward fault at Union City, California, *J. Geophys. Res. 101,* 6099-6108, 1996.

Lienkaemper, J. J., G. Borchardt, and M. Lisowski, Historic creep rate and potential for seismic slip along the Hayward fault, California, *J. Geophys. Res. 96,* 18,261-18,283, 1991.

Lienkaemper, J. J., and J. S. Galehouse, Revised long-term creep rates on the Hayward Fault, Alameda and Contra Costa Counties, California, *U.S. Geol. Surv., Open-File Rep. 97-690*, 18 p., 1997.
[http://quake.wr.usgs.gov:80/hazprep/NCEP/HF_creep/OF97_690dwnlod.html]

Lienkaemper, J.J., and P.L. Williams, New evidence in north Oakland of minor ground rupture on the Hayward fault and major rupturing in prehistoric earthquakes, *Geophys. Res. Lett.,* in press 1999.

Lienkaemper, J. J., P. L. Williams, P. Taylor, and K. Williams, New evidence of large surface-rupturing earthquakes along the northern Hayward fault zone, *SEPM (Society of Economic Paleontologists and Mineralogists) Pacific Section, 70th Annual Meeting, San Francisco, California, SEPM*, p. 38, 1995.

Lisowski, M., J. C. Savage, and W.H. Prescott, The velocity field along the San Andreas fault in central and southern California, *J. Geophys. Res. 96*, 8369-8390, 1991.

Louderback, G.D., Central California earthquakes of the 1830's, *Bull. Seismol. Soc. Am. 34*, 33-74, 1947.

Nowak D. J., Historical vegetation change in Oakland and its implications for urban forest management, *Journal of Arboriculture 19,* 313-319, 1993.

Oppenheimer, D. H., I. G. Wong, and F. W. Klein, The seismicity of the Hayward fault, California, *Calif. Div. of Mines and Geol. Spec. Publ. 113, 91-100,* 1993.

Radbruch, D. H. and Case, J. E., Preliminary geologic map of Oakland and vicinity, California, *U.S. Geological Survey Open-file Report* 67-183, 1967.

Savage, J. C., and M. Lisowski, Inferred depth of creep on the Hayward fault, central California, *J. Geophys. Res. 98*, 787-793, 1993.

Stuiver, M., and H. A. Polach, Discussion: Reporting of ^{14}C data, *Radiocarbon 19*, 355-363, 1977.

Stuiver, M., and P. J. Reimer, Extended ^{14}C database and revised CALIB radiocarbon calibration program, *Radiocarbon 35*, 215-230, 1993.

Toppozada, T. R., and G. Borchardt, Re-evaluation of the 1836 "Hayward Fault" earthquake and the 1838 San Andreas Fault earthquake, *Bull. Seismol. Soc. Am., 88*, 140-159.

Williams, P. L., Geologic record of southern Hayward fault earthquakes, *Calif. Div. of Mines and Geol. Spec. Publ. 113*, 171-179, 1993.

Working Group on California Earthquake Probabilities, Probabilities of large earthquakes occurring in the San Francisco Bay Region, California, *U.S. Geol. Surv., Circular 1053,* 51 p., 1990.

Working Group on Northern California Earthquake Potential, Database of potential sources for earthquakes larger than magnitude 6 in northern California *U.S. Geol. Surv., Open-File Rep. 96-705,* 53 p., 1996. [http://quake.wr.usgs.gov:80/hazprep/NCEP/]

Yu, E., and P. Segall, Slip in the 1868 Hayward earthquake from the analysis of historical triangulation data, *J. Geophys. Res. 101,* 16,101-16,118, 1996.

Appendix: Pollen analysis and age of gray clay, unit 28

Bulk wall samples taken during trenching at Mira Vista allowed for laboratory work on sedimentary pollen and organic content to determine whether the units surrounding the major erosional unconformity at the base of unit 28 are of historic age. We subsampled at 1-cm intervals a continuous section (see PS-3 at 6.2 m in trench 2 south wall, Fig. 5d) containing a 12-cm thick portion of unit 28 and a 4-cm thick portion of unit 25. Loss on ignition was performed to determine organic content, and standard acid digestion procedures (Faegri and Iversen, 1989) were used to prepare the samples for pollen analysis. After replacing sample depths with codes to ensure blind testing, all 16 samples were analyzed for organic content and scanned for non-native pollen types. In eight samples, four from each unit, at least 300 pollen grains were identified to the family, genus, or species level and plotted as a percentage of total aquatic or non-aquatic pollen. A total of 35 taxa were identified in the samples.

Figure A2 shows key results from laboratory work. We found no non-native pollen types in the unit below the unconformity. While this alone does not demonstrate a pre-historic age for the unit, the high organic content, abundance of *Sequoia* pollen, and relatively low levels of Poaceae and Brassicaceae pollen argue for a pre- or early-Spanish age for the unit (e.g. Byrne et. al., 1993). The presence of *Erodium* and *Eucalyptus* pollen throughout unit 28, above the unconformity, confirms that the unit is of historic age. *Erodium cicutarium* became naturalized in the San Francisco Bay Area soon after Spanish arrival in 1772 and is the likely source of the pollen (*Hendrey*, 1931; *Frankel*, 1967). *Erodium* at the base of unit 28 thus assigns an earliest date of 1772 to the sediments. *Eucalyptus* pollen throughout the top 3/4 of the unit imply a younger age for the majority of the unit. *Eucalyptus* species were not introduced to California until 1857 and were not planted in the East Bay until the 1870s (*Lanson*, 1952). The top 3/4 of the unit are thus assigned an age no earlier than 1870. However, it is quite possible that the bottom 1/4 of the unit is also post-1870, as *Eucalyptus* was not planted on a grand scale in the East Bay until the 1880s. The lower part of the gray clay unit is uniform in texture and lacks stratification, hence may suggest rapid deposition. Thus the appearance of a single grain of *Eucalyptus* pollen solely in the fourth of the lowest seven intervals may suggest only that the pollen density of *Eucalyptus* is quite low during this era. The sharp increases in Poaceae and Brassicaceae pollen in unit 28 reflect historic invasion of native, largely perennial grasslands by annual grasses and associated herbs. Other well-dated sites in the California coast ranges show marked increases in Poaceae and Brassicaceae pollen after 1860 (*Byrne et. al.,* 1993). The abrupt decline in *Sequoia* pollen in the gray unit is an expected result of widespread cutting of redwood stands in Oakland in the 1840s (*Gibbons,* 1893). The markedly lower organic content of unit 28 is likely due to grazing impacts on soils surrounding the site.

That unit 28 was deposited over a period of time and in an aquatic environment rather than as a massive fill event is supported by the aquatic pollen stratigraphy (Figure A3). Declining values of *Sagittaria* pollen and increasing values of Cyperaceae pollen are consistent with hydroseral succession in an infilling pond. Declining pollen concentration and organic content toward the top of the unit indicate an increasing sedimentary rate throughout the period of deposition, perhaps as a result of increasing grazing pressure. Pollen concentration at the bottom of the unit is roughly double that at the top, suggesting that the sedimentation rate doubled over the period of deposition.

In summary, unit 28 is firmly established to be of historic age, with the majority if not all of the sediments deposited after 1870 based on the occurrence of non-native *Eucalyptus* pollen. Although the base of the unit was not found to contain *Eucalyptus* pollen, the record of terrestrial tree and herb pollen is consistent with a late 19th century date of sediment

deposition. The aquatic pollen record, organic content, and pollen concentration in the unit indicate that it was not deposited as a massive fill but over time in a pond environment. The terrestrial pollen record in unit (?) below the unconformity suggest that the unit is pre- or early-Spanish (i.e. pre-1800). The amount of time represented by the unconformity is probably no less than 60 years (1800-1860). Sampling deeper in the gray clay is needed to determine more reliably the lowest stratigraphic level that contains *Eucalyptus* pollen.

Figure Captions

Figure 1. Location of trench site and other points along the Hayward fault. Currently known extent of 1868 surface rupture shown as solid gray band; dashed where subsurface extent of rupture is inferred. Stars indicate localities discussed in text. Creeping trace extends at least 68 km from P, Point Pinole to AC, Agua Caliente Creek. Trenching sites: MV, Mira Vista (*Hayward Fault Paleoearthquake Group*, 1997); MT, Montclair (*Lienkaemper et al.,* 1995); MH, Masonic Home (*Lienkaemper and Borchardt,* 1996); TP, Tule Pond (*Williams et al.,* 1993). Other localities: RM, Rocky Mound, key triangulation point of *Yu and Segall* (1996); BT, BART tunnel; CR, near Calaveras Reservoir, the branching point of northern Calaveras fault from faster-creeping southern Calaveras fault (Working Group on Northern California Earthquake Potential, 1996).

Figure 2. Orthophoto view of trench site on second fairway. Fault indicated by double dashes. Thick gray line shows approximate outline of sag pond; trench locations shown in detail in Figure 3.

Figure 3. Detailed topographic map of trench site. Hachured line shows extent of closed elevation contours, formerly a seasonal sag pond.

Figure 4. Logs of trenches showing area of detailed drafting (see Fig. 5). Darkest gray shading indicates weathered bedrock and colluvium derived from it. Light units are pond deposits that lie below thickest black line, which indicates major unconformity of historical age. Faults, principally near vertical, shown by intermediate line weights. Outside detail area, radiocarbon dates (uncalibrated yr BP) and sample numbers shown in boxes adjacent to samples (hexagons).

Figure 5. Detailed logs of trenches. Shading same as Figure 4. Ash-containing units 8, 15, 18 and 24 (u8, u15, u18, u24) shown with "v" pattern where ash is most concentrated (i.e., less disturbed). Units 1 through 31 (u1,...,u31), numbered in hexagons to distinguish from events 1 through 11 (i.e., paleoearthquakes, E1, ..., E11), numbered in squares. Fault traces numbered (e.g., F1, F2,...) to show approximate correlation across each trench and for discussion. Radiocarbon sample locations, marked by circles, show uncalibrated dates (in yr BP) and sample numbers. Heaviest solid line indicates major erosional unconformity underlying gray units (u28, u29). Next heaviest lines, mainly subhorizontal, indicate inferred approximate horizons at time of paleoearthquake ruptures. Intermediate line weights (mostly vertical) show fault traces: dashed where approximate, dotted where inferred, queried where uncertain. Colluvial units also labelled C1, C2, ...

Figure 6. Age constraints on paleoearthquakes. Event numbers shown above each event symbol, elongated ovals; calibrated age data given in Table 2. Age constraints all at 95% confidence, except event E11 (MRE) has upper bound limited by introduced pollen and pre-1776 historical limit of Toppozada and Borchardt (1998). Squares show ages of radiocarbon-dated units; weighted averages (method of Stuiver and Reimer, 1993) used wherever possible. P1, P2 and P3 indicate probability ranges described in Table 2.

Appendix Figure Captions

Figure A1. Trench logs showing field linework. Same description as for Fig. 5, but for clarity omits inferred event horizons and interpretative shading on stratigraphic units. Stratigraphic units, fault trace numbers and radiocarbon information kept to aid comparison.

Figure A2. Profile of unit 28 and unit25, showing variations in pollen frequencies and organic content. Dashed lines indicate sample positions, gray solid line indicates contact between units. Values for *Erodium* and *Eucalyptus* are numbers of grains found by scanning prepared slides, while values for Poaceae, Brassicaceae, and *Sequoia* are frequencies based on full (300+ grains) pollen counts.

Figure A3. Profile of unit 28 and unit 25, showing trends in organic content, pollen frequencies, and pollen concentration. Values for Sagittaria and Cyperaceae are based on full pollen counts and expressed as percent of total aquatic pollen. Aquatic pollen is defined here as including *Sagittaria*, Cyperaceae, *Typha latifolia*, *Typha/Sparganium*, and *Azolla*.

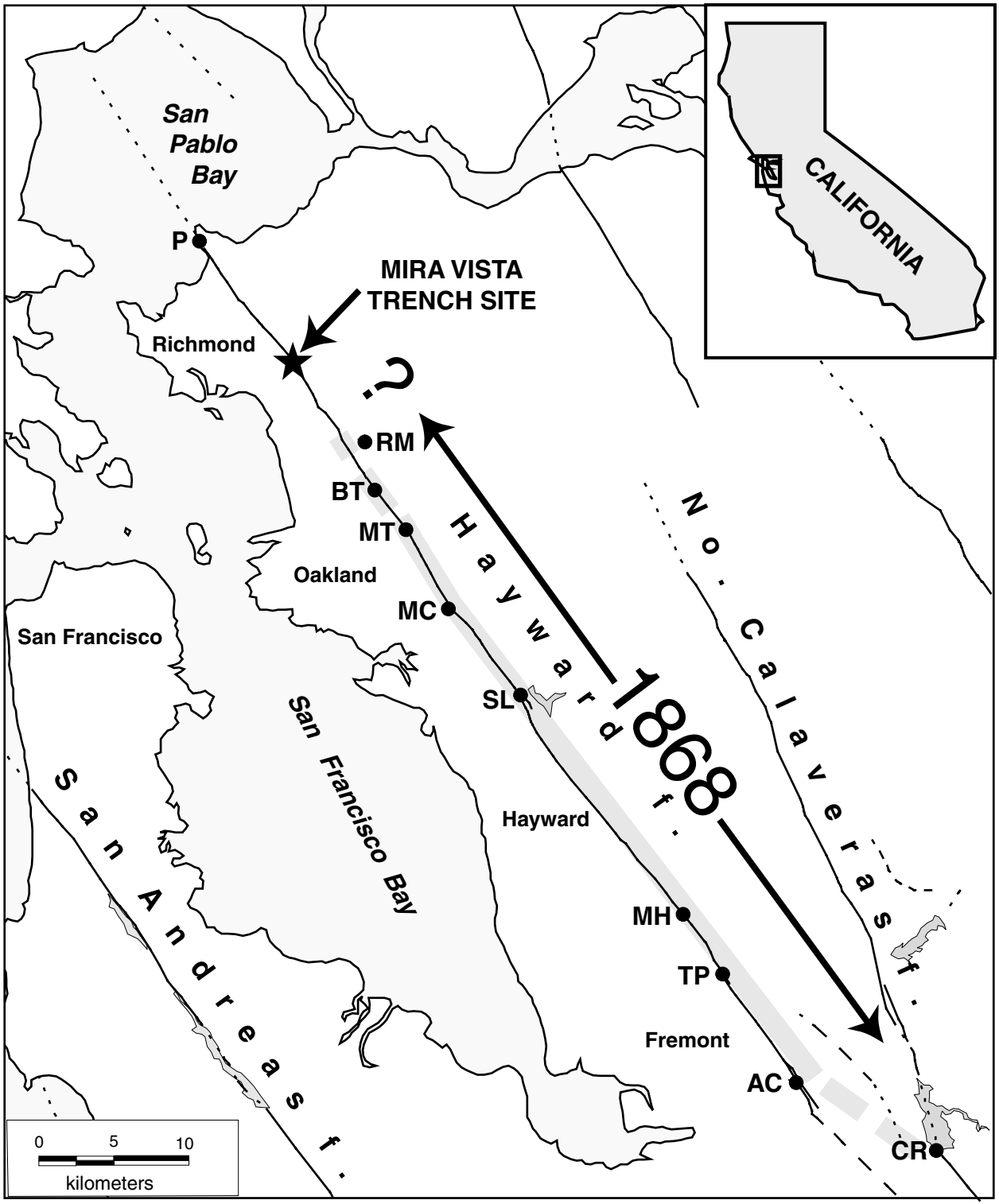
San Pablo Bay
P
MIRA VISTA TRENCH SITE
Richmond
?
RM
BT
MT
Oakland
MC
San Francisco
SL
Hayward f.
1868
No. Calaveras f.
San Francisco Bay
San Andreas f.
Hayward
MH
TP
Fremont
AC
CR
0 5 10
kilometers
CALIFORNIA

Figure 1

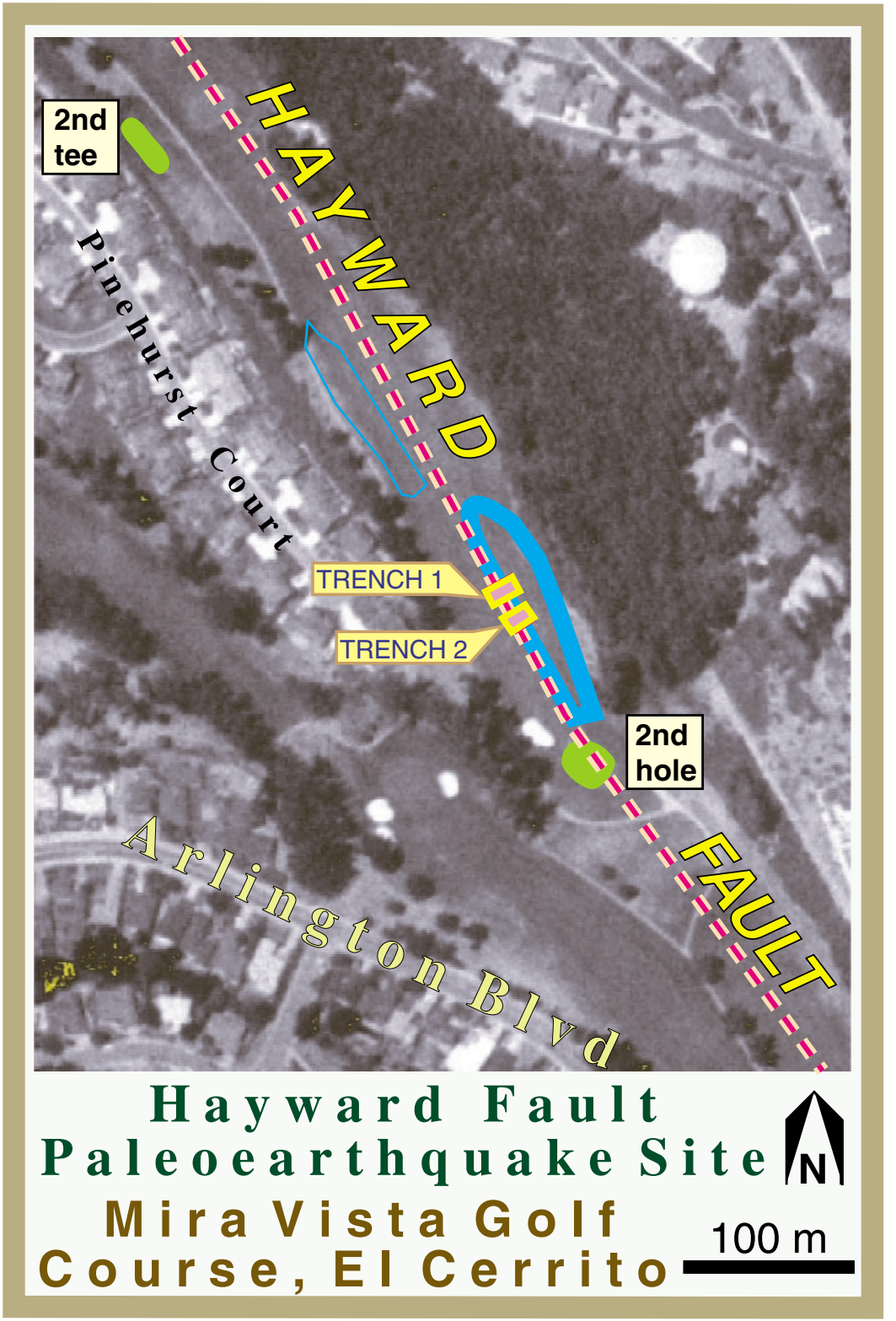
2nd tee
HAYWARD FAULT
Pinehurst Court
TRENCH 1
TRENCH 2
2nd hole
Arlington Blvd
Hayward Fault Paleoearthquake Site
Mira Vista Golf Course, El Cerrito
N
100 m

Figure 2

HAYWARD FAULT PALEO-EARTHQUAKE GROUP
SITE: MIRA VISTA GOLF & COUNTRY CLUB
HAYWARD FAULT
TRENCH 1
TRENCH 2
N
50 m
100 ft
20-cm contours

Figure 3

Figure 4a

Mira Vista trench 1

Log of north wall

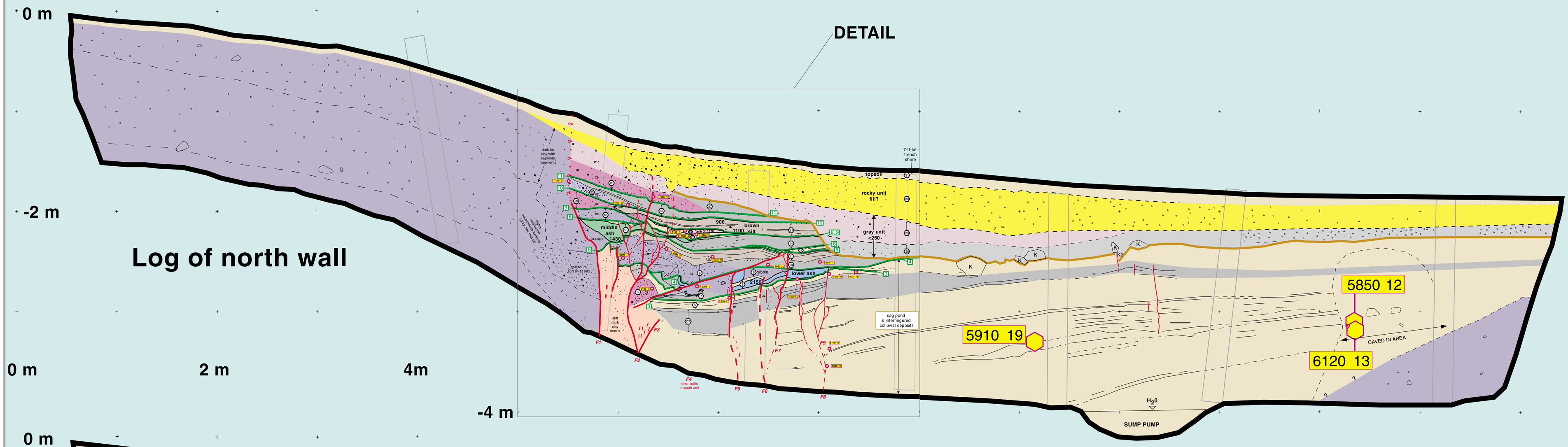

Log of south wall

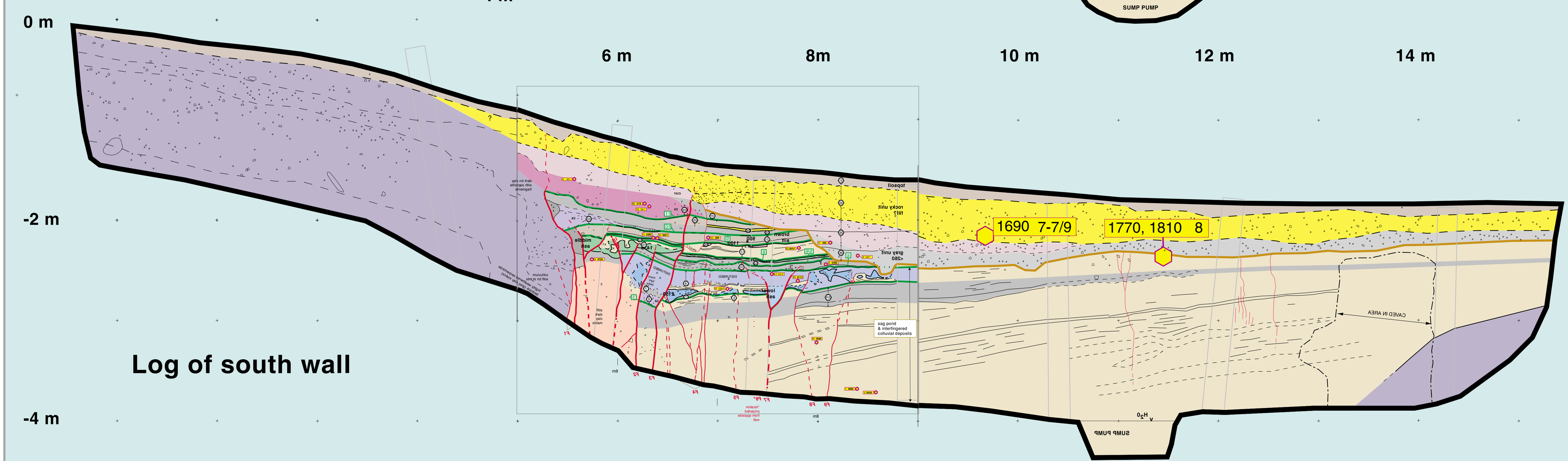

Figure 4b

Mira Vista trench 2

DETAIL

0 m

-2 m

Log of north wall

0 m

2 m

4 m

6 m

8 m

10 m

12 m

-4 m

2620 7

2130, 2090 8

2250 9

230 6

3700 5

H_2O

SUMP PUMP

0 m

-2 m

-4 m

CAVED IN AREA

Log of south wall

2110 1

2120 4

1960 5

SUMP PUMP

Figure 5a

Log of north wall, trench 1, Mira Vista trench site

symbol key

- fault trace
- radiocarbon age & sample number (years before 1950, uncalibrated; quotes on suspect dates)

"3070" 18

7-ft-tall trench shore

topsoil

rocky unit fill?

gray unit <260

brown silt

900

1100

dark bn clay with saprolite fragments

highly weathered serpentinite bedrock (gray clay matrix)

colluvium soft bn st mtx

stiff dark clay matrix

middle ash 1430

lower ash

rubble

2150

sag pond & interfingered colluvial deposits

"1130" 5

370 2

"1150" 22

1150 3

"ash 3" 1170

1190 24

1380 4

2000 8

"2120" 16

2390 1

2040 20

"2410" 11

"2980" 21

"3070" 18

3190 7

2240 9

2230 17

"3090" 14

5170 15

5600 10

C10 C9 C8 C7 C6 C5 C4 C4-C5(?) C2

F1 F2 F3 F4 F5 F6 F7 F8 F9

F4 minor faults in south wall

6m 8m

Figure 5b

Log of south wall, trench 1, Mira Vista trench site

symbol key

fault trace

radiocarbon age & sample number (years before 1950, uncalibrated; quotes on suspect dates)

"3070" 18

7-ft-tall trench shore

topsoil

rocky unit fill?

gray unit <260

brown silt

lower ash

middle ash

dark bn clay with saprolite fragments

colluvium soft bn st mtx

highly weathered serpentinite bedrock (gray clay matrix)

stiff dark clay matrix

sag pond & interfingered colluvial deposits

DISTURBED

many light blebs

no blebs

tan blebs

C10?

C9

C8

C3

900

1100

1430

2150

"ash 3"

FAULT ?

260 17

"760" 3

1440 23

2050 5

"2190" 14

2110 16

"2420" 13

4830 15

5940 2

5890 1

"150" 6

810 20

"190" 21

1040 10

1060 11

900 12

2070 4

F1 F2 F3 F4 F5 F6* F7 F8 F9

*location projected from opposite wall

6m

8m

Log of north wall, trench 2, Mira Vista trench site

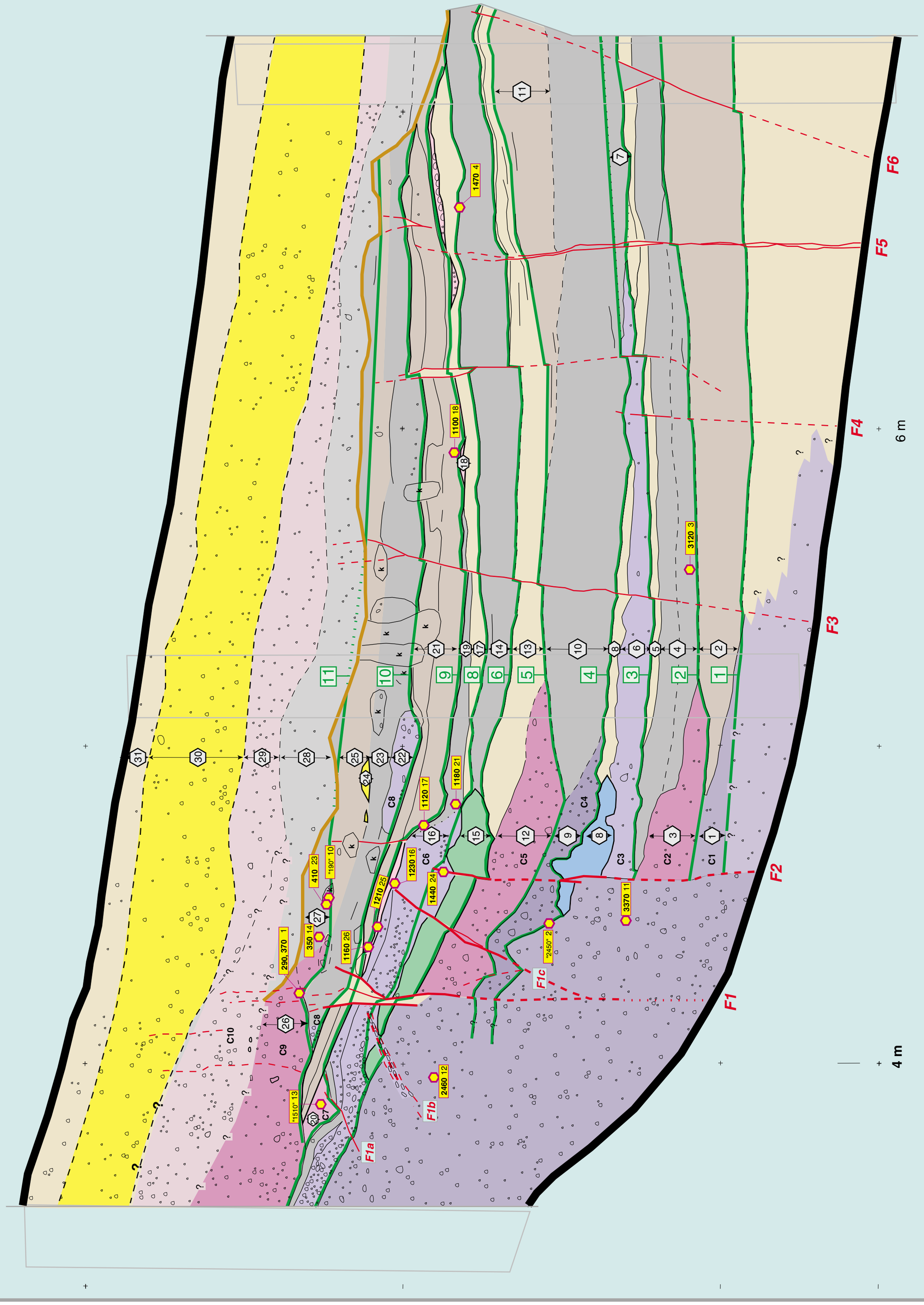

Figure 5c

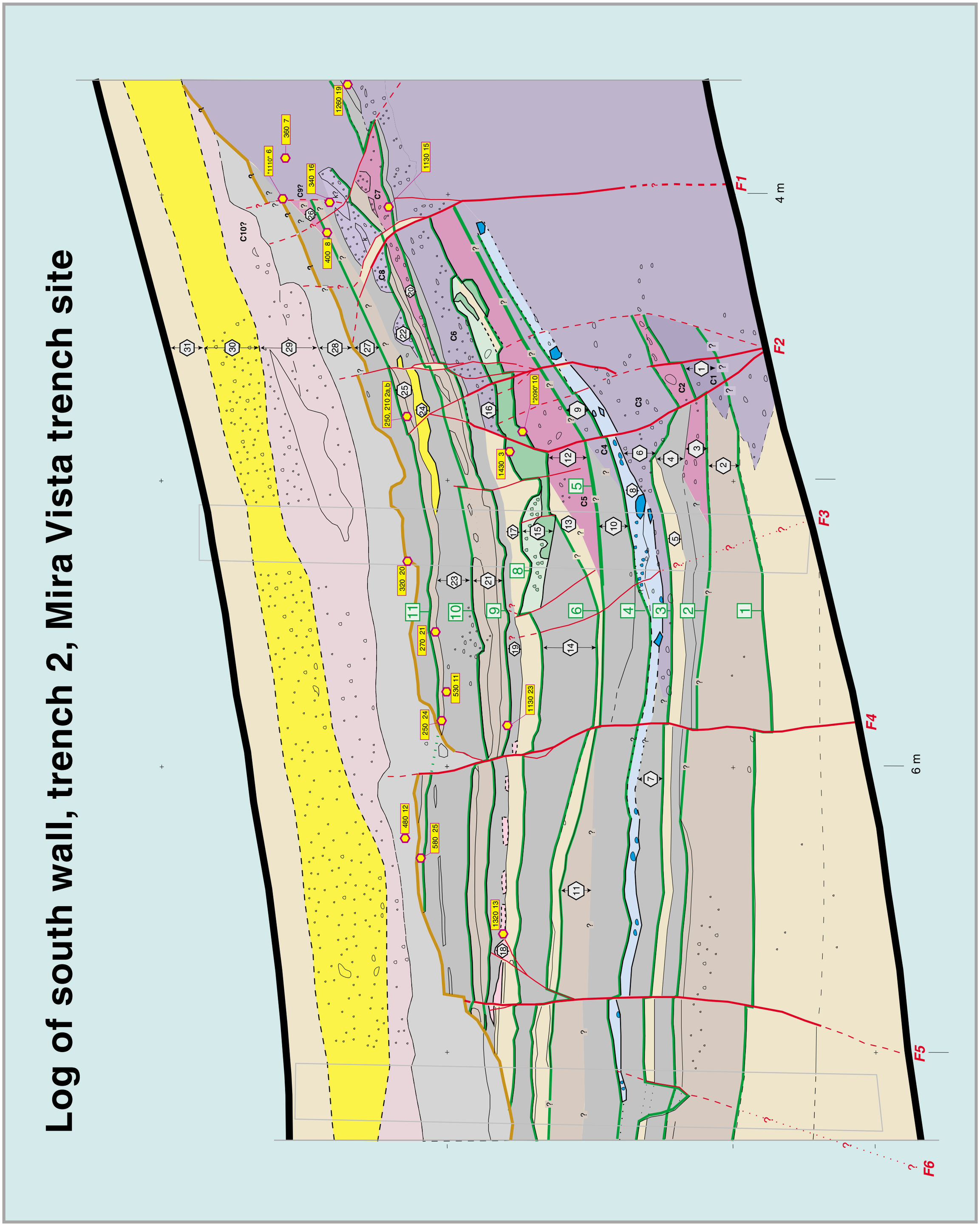
Log of south wall, trench 2, Mira Vista trench site
F1
F2
F3
F4
F5
F6
4 m
6 m
C1
C2
C3
C4
C5
C6
C7
C8
C9?
C10?
1260 19
360 7
"1110" 6
340 16
400 8
1130 15
"2090" 10
250, 210 2a,b
1430 3
320 20
270 21
530 11
1130 23
250 24
480 12
580 25
1320 13

Figure 5d

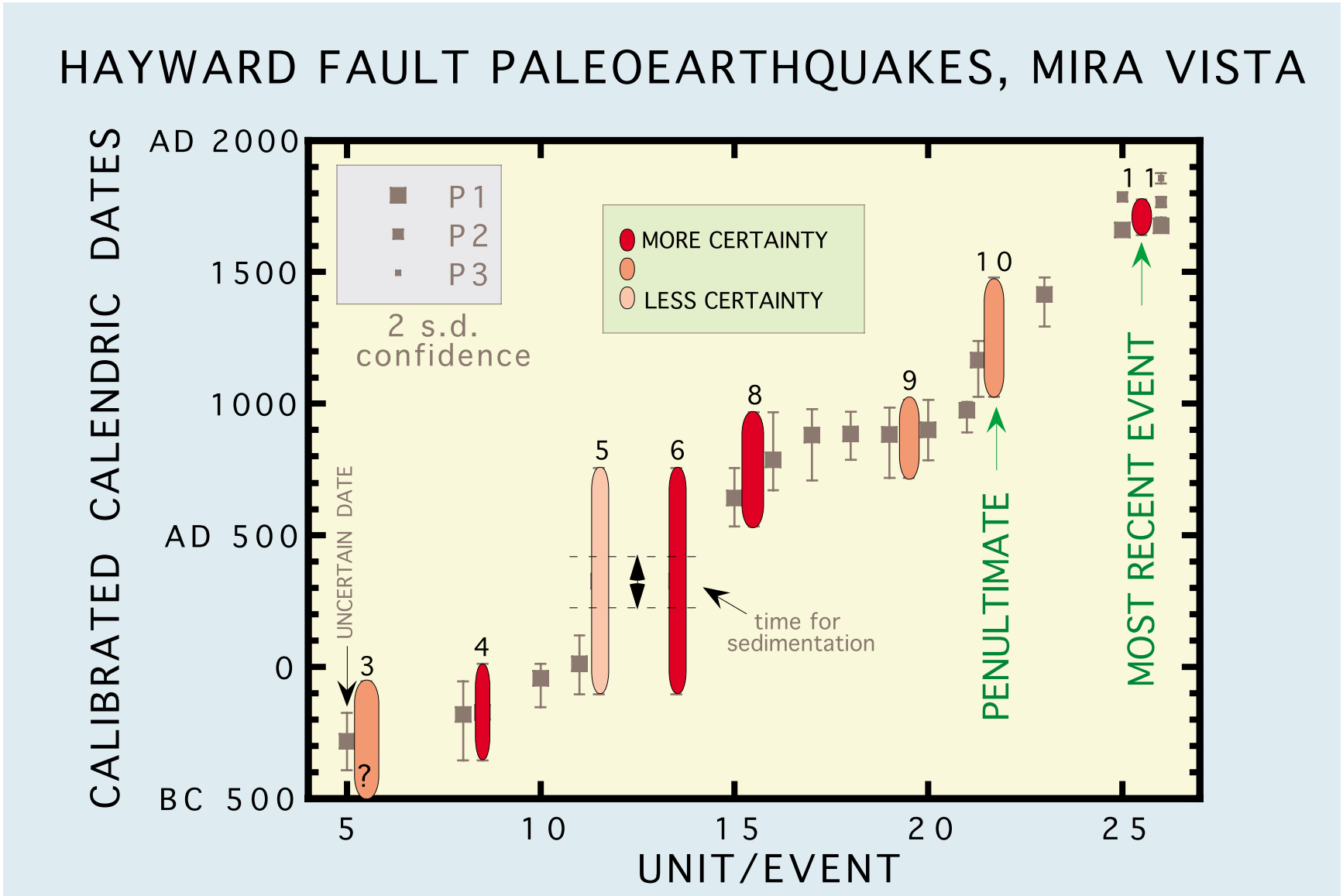
HAYWARD FAULT PALEOEARTHQUAKES, MIRA VISTA
CALIBRATED CALENDRIC DATES
AD 2000
1500
1000
AD 500
0
BC 500
5
10
15
20
25
UNIT/EVENT
P1
P2
P3
2 s.d. confidence
MORE CERTAINTY
LESS CERTAINTY
UNCERTAIN DATE
?
3
4
5
6
8
9
10
11
time for sedimentation
PENULTIMATE
MOST RECENT EVENT

Figure 6

Figure A1a

Trench 1, north wall, DETAIL

dark bn clay with saprolite fragments

highly weathered serpentinite bedrock (gray clay a matrix)

colluvium soft bn st mtx

stiff dark clay matrix

7-ft-tall trench shore

topsoil

fill

gray unit

Brown silt

900

1100

rubble

sag pond & interfingered colluvial deposits

"1130" 5

"1150" 22

370 2

1150 3

1380 4

1190 24

2000 8

"2120" 16

2390 1

2040 20

"2410" 11

"2980" 21

"3070" 18

3190 7

2240 9

"3090" 14

2230 17

5170 15

5600 10

C10

C9

C8

C7

C6

C4-C5(?)

C4

C2

A2

A3

A1

2/4

F1

F2

F3

F4

minor faults in south wall

F5

F6

F7

F8

F9

6m

8m

Figure A1b

Trench 1, south wall, DETAIL

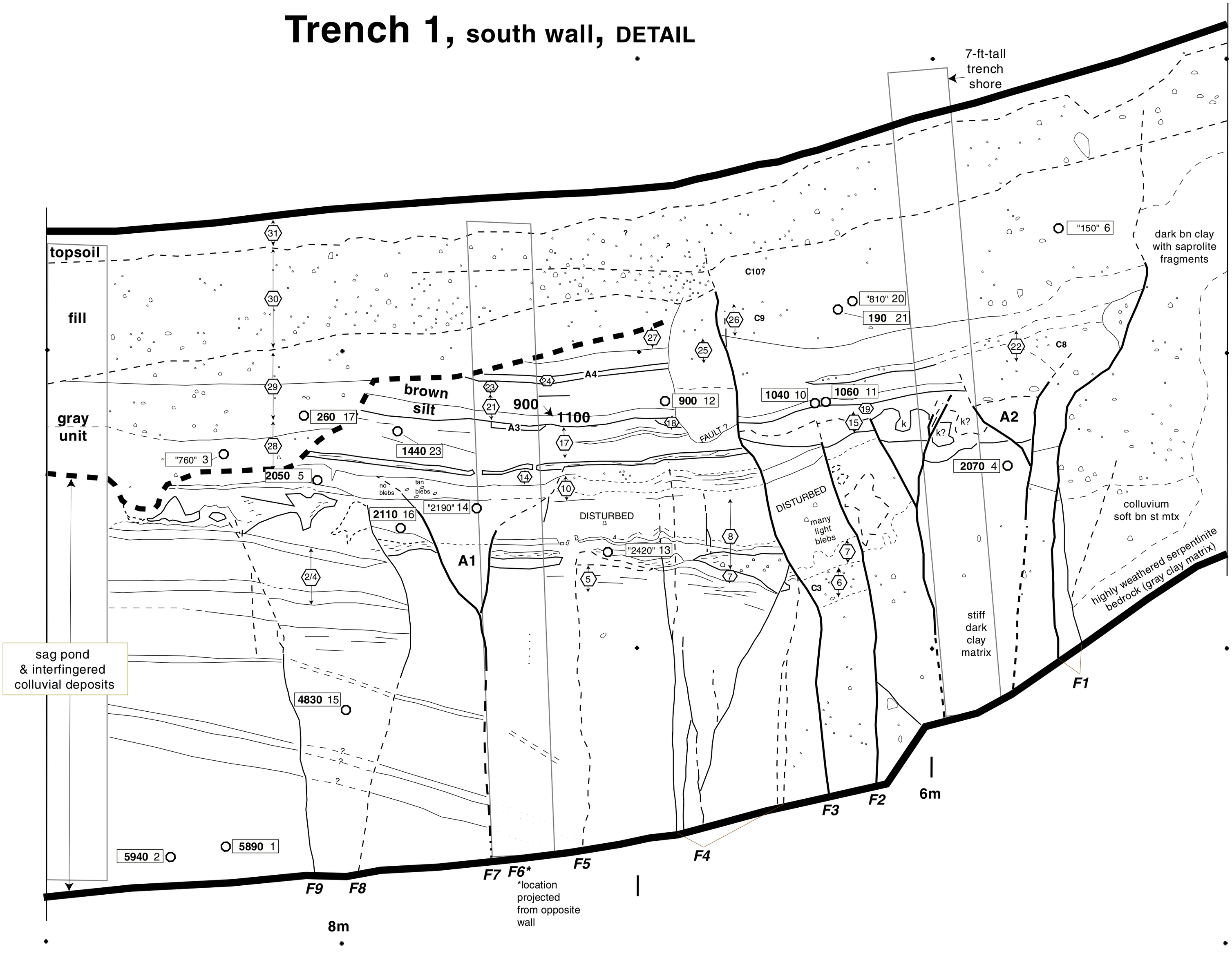

Figure A1c

Trench 2, north wall, DETAIL

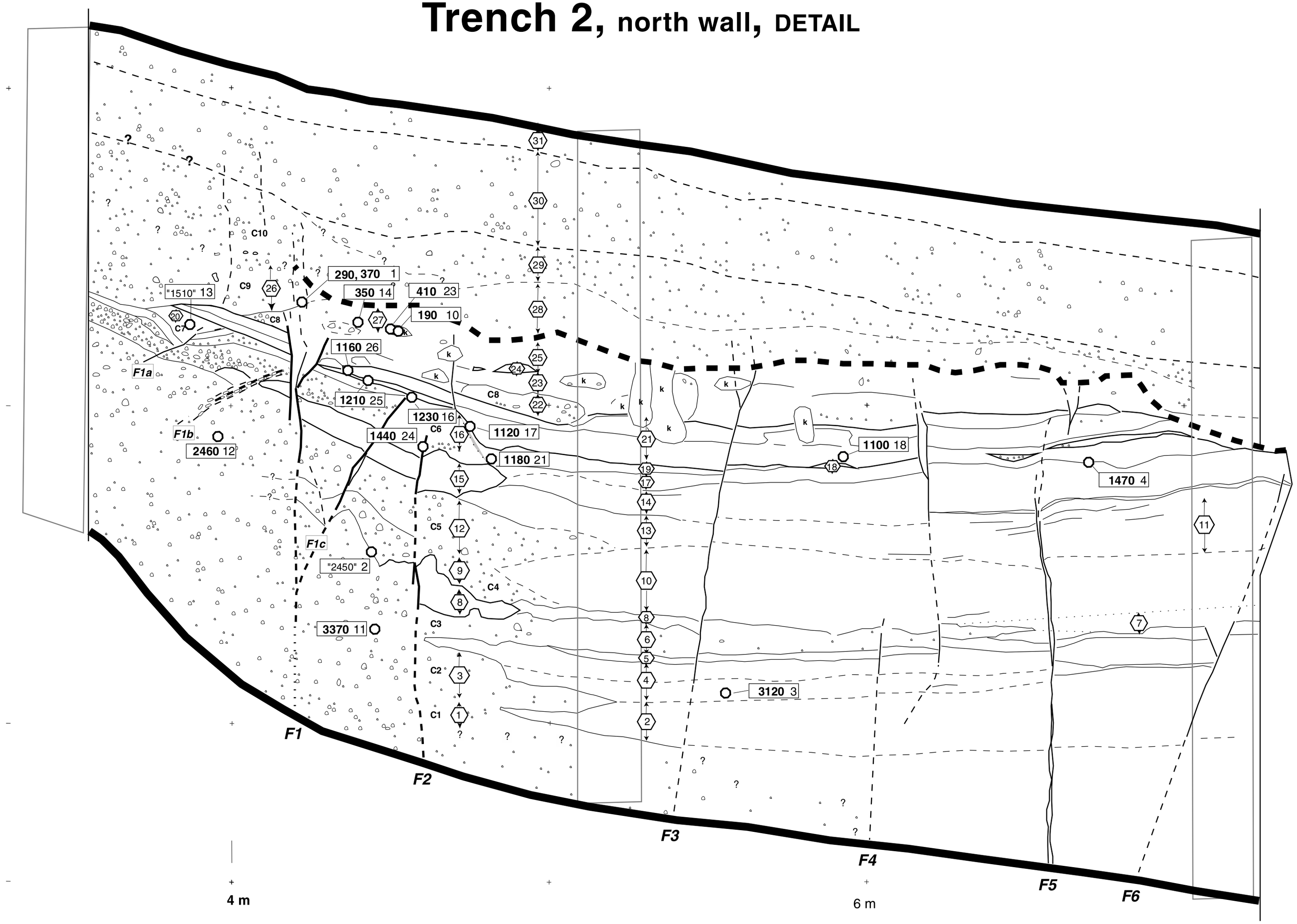

Figure A1d

Trench 2, south wall, DETAIL

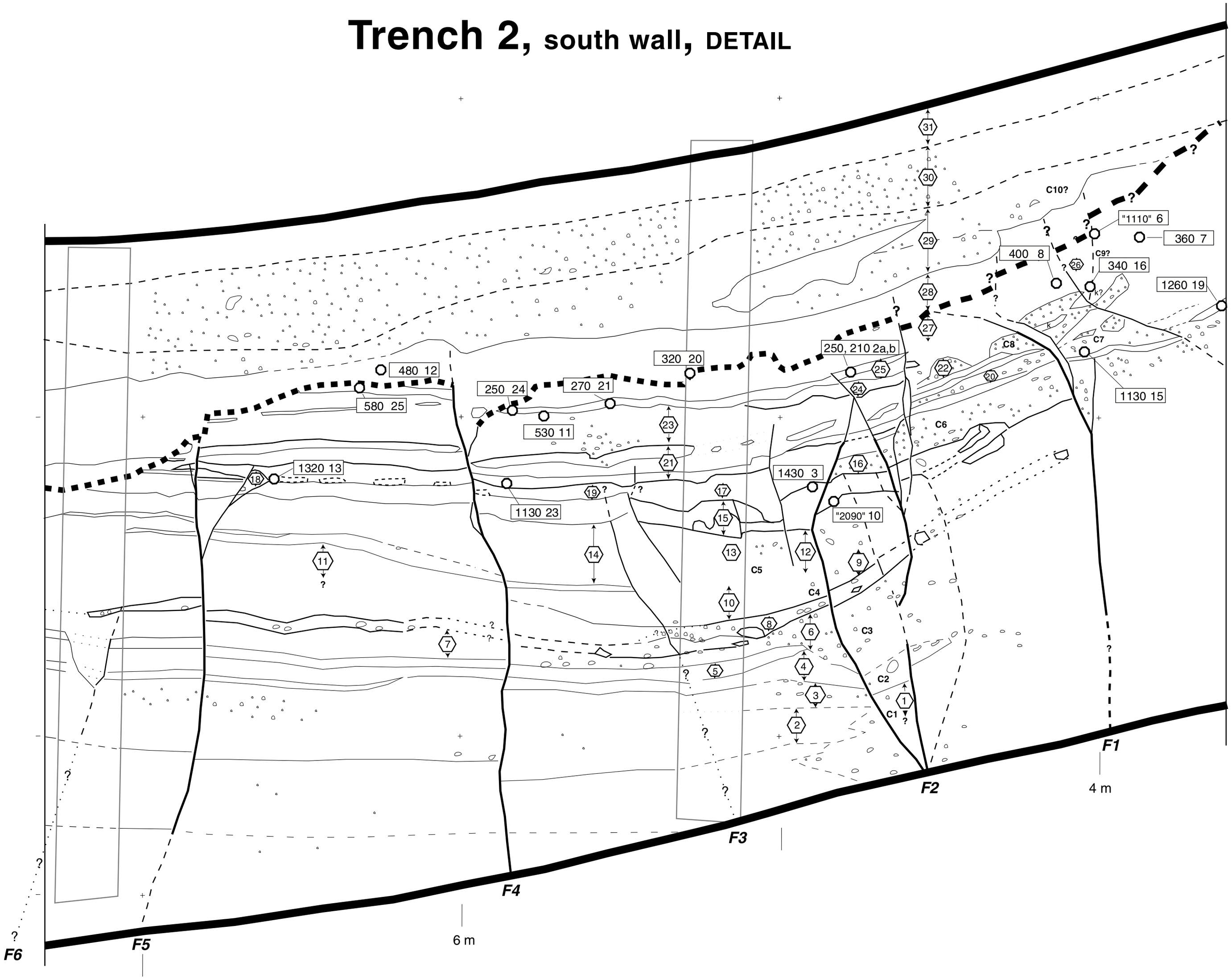

Figure A2

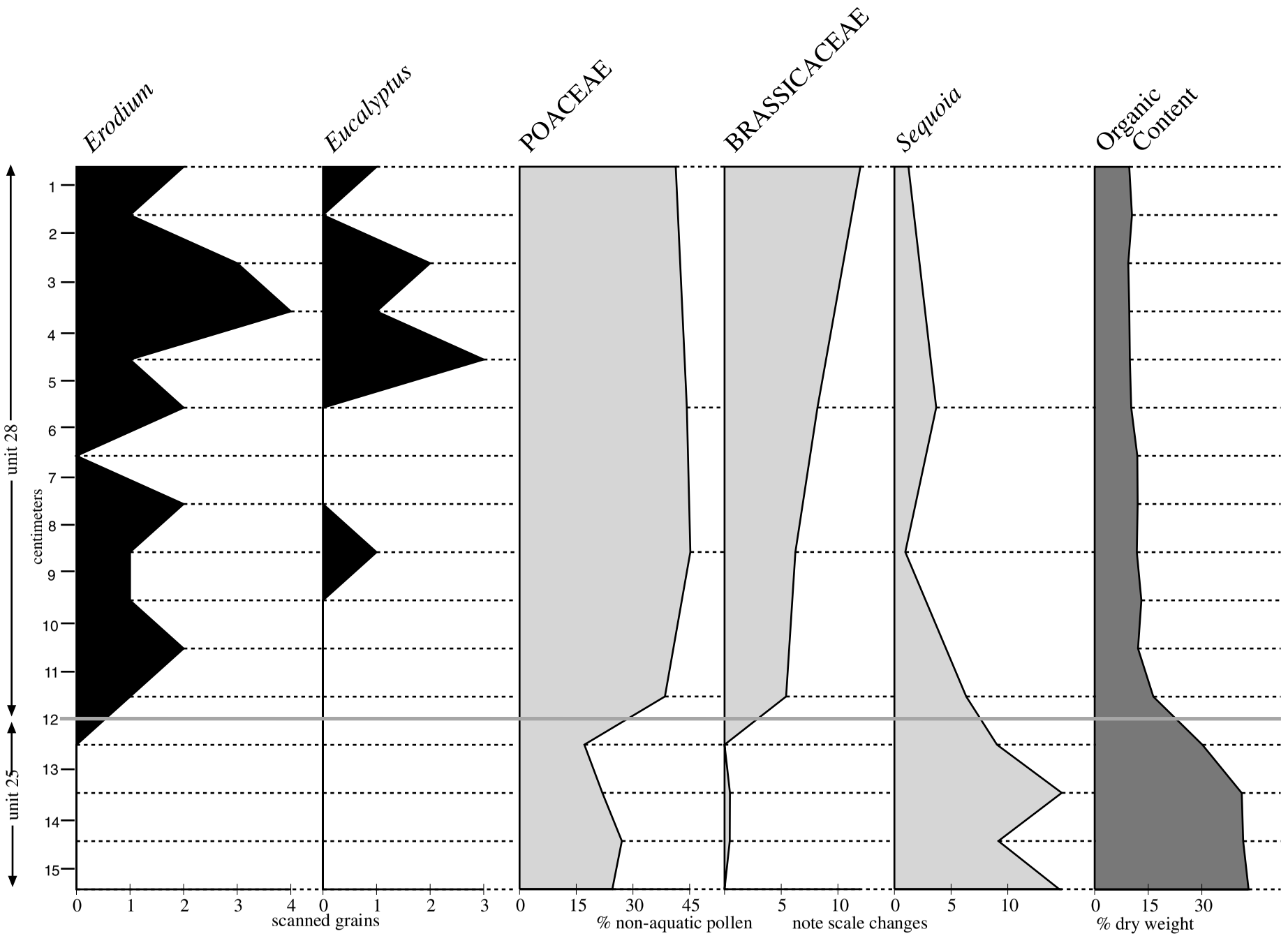
MIRA VISTA SELECTED POLLEN AND LOSS ON IGNITION
Erodium
Eucalyptus
POACEAE
BRASSICACEAE
Sequoia
Organic Content
unit 28
unit 25
centimeters
1
2
3
4
5
6
7
8
9
10
11
12
13
14
15
0 1 2 3 4
0 1 2 3
scanned grains
0 15 30 45
% non-aquatic pollen
5 10
note scale changes
0 5 10
0 15 30
% dry weight

Figure A3

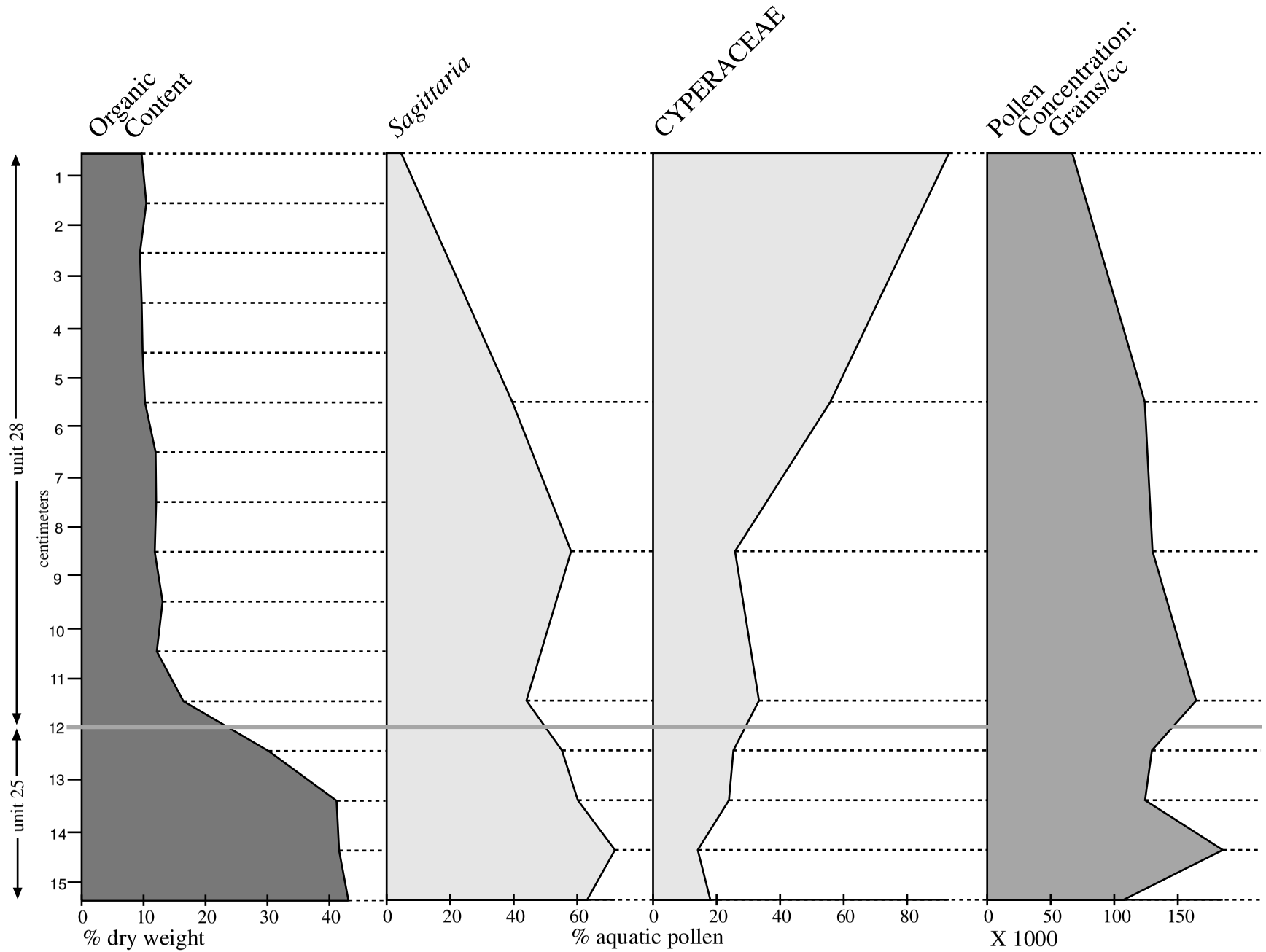
MIRA VISTA SELECTED AQUATIC POLLEN AND LOSS ON IGNITION
Organic Content
Sagittaria
CYPERACEAE
Pollen Concentration: Grains/cc
unit 28
unit 25
centimeters
1
2
3
4
5
6
7
8
9
10
11
12
13
14
15
0 10 20 30 40
% dry weight
0 20 40 60
0 20 40 60 80
% aquatic pollen
0 50 100 150
X 1000

Table 1. Evidence for paleoearthquakes.

EVENT	more certainty	intermediate certainty	less certainty
11	[2s]: on faults F1 & F2 more deformation below top of u25	[2n]: folding in u23	[1n]: C9, fault termination [1s]: C9, u23 ends abruptly at fault F1 [2n]: C9, 4 weak fault terminations & fissure fill [2s]: probable C9 & fault termination
10	[1n & 1s]: much more deformation below u23 near F2 and westward	[1s]: abrupt terminations of pond sediments (u21) & faulting covered and infilled by C8	[1n,1s,2n,2s]: C8 colluvium [2s]: fault termination [1s]: 2 fault terminations
9	[2s]: 3 extremely distinct fault terminations below u21	[2n]: much more deformation below u21 (folding between faults F1a & F1b)	[1n,2n,2s]: C9 colluvium [2n]: 2 fault terminations
8	[1s, 2s]: strong deformation of u15 (ash 2)	[1n]: 2 distinct fault terminations	[2n, 2s]: C6, large, distinct colluvium [2n]: 2 fault terminations [1s]: 4 fault terminations
6	[1n]: 3 distinct fault terminations & "thrust" faulting between & above F5 to F7	[1s]: u10 much more deformed (folded above fault F4) than u14 (flat-lying)	[2s]: 2 fault terminations [2n,2s]: fault termination
5	[1n]: abrupt fault termination & u11 much more deformed than u13	[2n, 2s]: C5, large & distinct colluvium at event horizon	
4	[1n,1s,2n,2s]: intense deformation of u8 (ash 1)	[1n]: major "thrust" faulting [1s]: u8 (ash 1) in fissure	[1n,2n,2s]: C4 colluvium [1n,1s]: 3 fault terminations in each wall

Abbreviations: [1n, 1s, ...], trench 1 north wall, south wall; u1, u2, ..., unit 1, 2, ...

Table 2. Calibrated calendric dates (AD positive) and 95% probability ranges for units and paleoearthquakes (events).

UNIT or EVENT	P1L	P1U	P2L	P2U	P3L	P3U	Comment
u26	1652	1706	1713	1821	1837	1876	Sum of P1 (25.6%) + P2 (62.8%) + P3 (7.0%) = 95.4%
E11	**1640**	**1776**					Most recent event. P1U, historical age constraint after Toppazada and Borchardt (1998)
u25	1640	1679	1768	1802			Sum of P1 (61.3%) + P2 (34.1%) = 95.4%
u23	1300	1479					Ash 4 is u24
E10	**1027**	**1479**					
u21b	1027	1238					
u21a	892	1008					
u20	785	1014					
E9	**718**	**1014**					
u19	718	985					
u18	784	967					Ash 3
u17	708	979					
u16	667	968					
E8	**534**	**968**					
u15	534	756					Ash 2
E6	**-104**	**756**					
E5	**-104**	**756**					
u11	-104	121					
u10	-152	13					
E4	**-355**	**13**					
u8	-355	-54					Ash 1
E3	**-392**	**-54**					
u5	-392	-173					Age of u5 needs verification, much older dates also possible.

Note: Calibrated age ranges P1L to P1U represent 2 standard deviations calculated with program of Stuiver and Reimer (1993) except for units 25-26 for which multiple intercepts exist in calibration curve, see comment column above for probabilities associated with each intercepted age range.

Table A1. Radiocarbon data

CAMS #	Sample name	^{14}C age (yr BP)	±	Unit		Calibrated age (cal yr) (2σ)	d13C	Fraction Modern	±	D14C	±
38508	1S-07-7/9	1690	60	*30*		fill	-26.0	.8107	.0054	-189.3	5.4
38509	2N-07	2620	70	*30*		"	-26.0	.7219	.0055	-278.1	5.5
38511	1S-17	260	50	*28*		historical pond, gray clay unit,	-25.9	.9680	.0051	-32.0	5.1
38512	2S-20	320	70	*28*		see appendix	-26.0	.9615	.0075	-38.5	7.5
38513	2S-12	480	50	*28*		on pollen	-25.7	.9423	.0052	-57.7	5.2
38514	1S-03	760	50	*28*		analysis	-26.0	.9094	.0051	-90.6	5.1
						Major historical-aged unconformity					
38515	2N-10	190	50	*27*	k	––	-25.0	.9766	.0054	-23.4	5.4
38516	2N-14	350	40	*27*		––	-26.4	.9577	.0044	-42.3	4.4
38517	2N-23	410	80	*27*	k	––	-28.7	.9501	.0092	-49.9	9.2
38518	2S-06	1110	90	*27*	?	––	-26.0	.8706	.0090	-129.4	9.0
38510	1S-06	150	50	*26*	?	––	-26.9	.9810	.0055	-19.0	5.5
38519	1S-21	**190**	40	***26***		1652-1706 (26%) 1713-1821 (63%) 1837-1876 (7%)	-25.7	.9770	.0048	-23.0	4.8
38543	2N-01	290	40	*26*		––	-26.1	.9643	.0043	-35.7	4.3
38544	2S-07	360	70	*26*	?	––	-29.5	.9560	.0079	-44.0	7.9
38545	1N-02	370	50	*26*		––	-26.7	.9554	.0053	-44.6	5.3
38546	2N-01 repeat	370	50	*26*		––	-26.1	.9555	.0054	-44.5	5.4
38547	1S-20	800	120	*26*		––	-26.0	.9047	.0127	-95.3	12.7
38548	2S-02 repeat	**210**	50	***25***	wa	1640-1679 (61%) 1768-1802 (34%)	-26.0	.9743	.0055	-25.7	5.5
38549	2S-02	**250**	50	***25***	wa	"	-26.0	.9691	.0054	-30.9	5.4
38551	2S-24	**250**	40	***25***	wa	"	-26.8	.9699	.0042	-30.1	4.2
38552	2S-21	270	150	*25*		(±150 yr age err.)	-26.0	.9666	.0169	-33.4	16.9
38553	2S-16	340	60	*25*	?	––	-26.4	.9586	.0060	-41.4	6.0
38554	2S-08	390	40	*25*	?	––	-26.0	.9528	.0044	-47.2	4.4
38556	2S-25	580	80	*25*		––	-26.0	.9300	.0084	-70.0	8.4
38555	2S-11	**530**	70	***23***		AD 1294-1496	-26.0	.9362	.0075	-63.8	7.5
38557	1N-22	1150	50	*23*		––	-26.0	.8671	.0044	-132.9	4.4
38558	1N-05	1130	50	*22*	?	––	-26.0	.8683	.0049	-131.7	4.9
38502	1S-12	**900**	50	***21b***		AD 1027-1479	-26.0	.8944	.0052	-105.6	5.2
38503	1S-10	**1040**	50	***21a***	wa	AD 892-1008	-26.0	.8782	.0050	-121.8	5.0
38504	1S-11	**1060**	60	***21a***	wa	"	-26.0	.8758	.0060	-124.2	6.0
38505	2N-18	**1100**	50	***21a***	wa	"	-26.0	.8723	.0052	-127.7	5.2
38506	2N-17	**1120**	40	***21a***	wa	"	-26.0	.8699	.0040	-130.1	4.0
38507	2S-23	**1130**	50	***21a***	wa	"	-26.0	.8683	.0048	-131.7	4.8
38559	2S-15	**1130**	50	***20***		AD 785-1014	-26.0	.8683	.0048	-131.7	4.8
38560	2N-13	1510	120	*20*		––	-26.0	.8286	.0116	-171.4	11.6
38561	2N-21	**1180**	50	***19***		AD 718-985	-26.0	.8637	.0047	-136.3	4.7
38562	2S-19	1260	100	*19*		––	-26.0	.8551	.0103	-144.9	10.3
38617	1N-03	**1150**	50	***18***	wa	AD 784-967	-25.8	.8664	.0048	-133.6	4.8
38618	2N-26	**1160**	50	***18***	wa	"	-26.0	.8656	.0048	-134.4	4.8

Table A1. Radiocarbon data (continued)

CAMS #	Sample name	^{14}C age (yr BP)	±	Unit		Calibrated age (cal yr) (2σ)	d13C	Fraction Modern	±	D14C	±
38619	2N-25	**1210**	50	***18***	wa	"	-26.0	.8597	.0048	-140.3	4.8
38620	2S-13	1320	50	*18*		––	-26.0	.8483	.0047	-151.7	4.7
38621	1N-24	**1190**	50	***17***		AD 708-979	-26.0	.8619	.0050	-138.1	5.0
38622	1N-04	1380	50	*17*		––	-26.0	.8419	.0046	-158.1	4.6
38623	1S-23	1440	50	*17*		––	-26.0	.8361	.0049	-163.9	4.9
38624	2N-04	1470	50	*17*	?	––	-26.0	.8332	.0047	-166.8	4.7
38625	2N-16	**1230**	60	***16***		AD 667-968	-26.0	.8580	.0058	-142.0	5.8
38626	2N-24	1440	60	*16*		––	-26.0	.8360	.0053	-164.0	5.3
38627	2S-03	**1430**	70	***15***		AD 534-756	-26.0	.8367	.0072	-163.3	7.2
38628	2S-10	2090	60	*15*		––	-26.0	.7711	.0054	-228.9	5.4
38629	1S-08	1770	50	*13*	?	––	-26.0	.8025	.0041	-197.5	4.1
38630	1S-08 repeat	1810	60	*13*	?	––	-26.0	.7986	.0054	-201.4	5.4
38631	2N-12	2460	50	*12*	?	––	-26.0	.7358	.0041	-264.2	4.1
38632	1N-08	**2000**	50	***11***		104 BC - AD 121	-26.0	.7792	.0042	-220.8	4.2
38633	1N-16	2120	50	*11*		––	-26.0	.7684	.0042	-231.6	4.2
38634	2N-09	2250	60	*11*	k	––	-26.0	.7561	.0053	-243.9	5.3
38635	2N-06	230	40	*10*	k	––	-26.0	.9716	.0046	-28.4	4.6
38636	1N-20	**2040**	50	***10***	wa	152 BC - AD 13	-26.0	.7760	.0046	-224.0	4.6
38637	1S-05	**2050**	50	***10***	wa	"	-26.0	.7746	.0043	-225.4	4.3
38638	1S-04	**2070**	40	***10***	wa	"	-27.9	.7729	.0035	-227.1	3.5
38639	2N-08 repeat	2090	50	*10*	k	––	-26.0	.7709	.0046	-229.1	4.6
38640	2S-01	2110	50	*10*	?	––	-26.0	.7694	.0043	-230.6	4.3
38641	2S-04	2120	50	*10*	?	––	-26.0	.7684	.0043	-231.6	4.3
38642	2N-08	2130	50	*10*	k	––	-26.0	.7667	.0044	-233.3	4.4
38643	1N-11	2410	70	*10*		––	-26.0	.7411	.0057	-258.9	5.7
38644	1N-01	2390	50	*9*		––	-25.3	.7428	.0042	-257.2	4.2
38645	2N-02	2450	50	*9*	?	––	-26.0	.7373	.0042	-262.7	4.2
39123	1S-16	**2110**	50	***8***	wa	355 BC - 54 BC	-26.0	.7688	.0045	-231.2	4.5
39124	1S-14	**2190**	50	***8***	wa	"	-26.0	.7613	.0040	-238.7	4.0
39125	1N-09	2240	40	*8*		––	-26.0	.7571	.0038	-242.9	3.8
39126	1S-13	2420	50	*8*		––	-26.0	.7402	.0041	-259.8	4.1
39127	1N-14	3090	50	*7*		––	-26.0	.6810	.0037	-319.0	3.7
39128	1N-17	**2230**	50	***5***		392 BC- 173 BC	-26.0	.7572	.0042	-242.8	4.2
39129	1N-21	2980	50	*5*		––	-26.0	.6901	.0040	-309.9	4.0
39130	1N-18	3070	50	*5*		––	-26.0	.6825	.0038	-317.5	3.8
39131	2S-05	1960	60	*4*	?	––	-29.6	.7831	.0054	-216.9	5.4
39132	2N-03	3120	50	*4*		1464 BC - 1261 BC	-26.0	.6781	.0038	-321.9	3.8
39133	1N-07	3190	50	*3*		1526 BC - 1323 BC	-26.0	.6725	.0038	-327.5	3.8
39134	2N-11	3370	50	*3*	?	––	-26.0	.6573	.0038	-342.7	3.8
39135	2N-05	3700	50	*2*		2203 BC - 1928 BC	-26.0	.6310	.0035	-369.0	3.5
39136	1S-15	4830	50			3703 BC - 3389 BC	-26.0	.5482	.0032	-451.8	3.2
39137	1N-15	5170	50			4210 BC - 3911 BC	-26.0	.5257	.0029	-474.3	2.9
39138	1N-10	5600	50			4533 BC - 4344 BC	-26.0	.4982	.0029	-501.8	2.9

Table A1. Radiocarbon data (continued)

CAMS #	Sample name	^{14}C age (yr BP)	±	Unit	Calibrated age (cal yr) (2σ)	Fraction d13C	Modern	±	D14C	±
39139	1N-12	5850	50		(caved after sampling, location ± 0.5? m)	-26.0	.4829	.0029	-517.1	2.9
39140	1S-01	5890	40	wa	4843 BC - 4722 BC	-26.3	.4801	.0023	-519.9	2.3
39141	1N-19	5910	50	wa	"	-26.0	.4790	.0027	-521.0	2.7
39142	1S-02	5940	50	wa	"	-26.0	.4773	.0027	-522.7	2.7
39143	1N-13	6120	60		(caved after sampling, location ± 0.5? m)	-26.0	.4670	.0030	-533.0	3.0
39144	1S-07 7/8	6230	50		(caved after sampling, location highly uncertain)	-26.0	.4605	.0025	-539.5	2.5

1) Delta 13C values are the assumed values according to Stuiver and Polach (Radiocarbon, v. 19, p.355, 1977) when given without decimal places. Values measured for the material itself are given with a single decimal place.

2) The quoted age is in radiocarbon years using the Libby half life of 5568 and following the conventions of Stuiver and Polach (ibid.).

3) Radiocarbon concentration is given as fraction Modern, D14C, and conventional radiocarbon age.

4) Sample preparation backgrounds have been subtracted, based on measurements of samples of 14C-free coal. Backgrounds were scaled relative to sample size.

5) Letter codes used: k = krotovina, sampled from infilled burrow; wa = included in weighted average for unit; ? = unit identity highly uncertain

6) Calibrated ages computed only for samples identified as being in stratigraphic sequence and having meaningfull ages. Some ages are clearly rejectable based on having prehistoric radiocarbon in historical-aged units, others are judged inconsistent for appearing to be out of sequence by more than 100 yr.

Table A2. Loss on ignition data for unit 28 and unit below unconformity

Sample interval	cruc empty	cruc+wet sed	wet sed	cruc + dry sed	dry sed	cruc + min	min	LOI
0-1 cm	8.8588	9.9836	1.1248	9.6752	0.8164	9.5962	0.7374	9.68%
1-2 cm	8.6387	9.7713	1.1326	9.4411	0.8024	9.3573	0.7186	10.44%
2-3 cm	8.6279	9.7973	1.1694	9.4813	0.8534	9.4010	0.7731	9.41%
3-4 cm	7.5164	8.6386	1.1222	8.3214	0.8050	8.2434	0.7270	9.69%
4-5 cm	8.7828	9.9004	1.1176	9.5753	0.7925	9.4972	0.7144	9.85%
5-6 cm	8.9256	10.0496	1.1240	9.7856	0.8600	9.6976	0.7720	10.23%
6-7 cm	8.2910	9.3823	1.0913	8.9943	0.7033	8.9103	0.6193	11.94%
7-8 cm	8.0705	9.1227	1.0522	8.7514	0.6809	8.6695	0.5990	12.03%
8-9 cm	8.2242	9.3438	1.1196	8.9563	0.7321	8.8699	0.6457	11.80%
9-10 cm	8.8529	9.9797	1.1268	9.5642	0.7113	9.4712	0.6183	13.07%
10-11 cm	8.9223	10.0768	1.1545	9.6798	0.7575	9.5879	0.6656	12.13%
11-12 cm	8.7139	9.7958	1.0819	9.3402	0.6263	9.2373	0.5234	16.43%
12-13 cm	8.8465	9.6773	0.8308	9.2058	0.3593	9.0974	0.2509	30.17%
13-14 cm	8.6720	9.4298	0.7578	8.9072	0.2352	8.8104	0.1384	41.16%
14-15 cm	6.9804	7.7685	0.7881	7.2342	0.2538	7.1287	0.1483	41.57%
15-16 cm	8.4559	9.1999	0.7440	8.6964	0.2405	8.5928	0.1369	43.08%

All weights in grams

Table A3. Pollen scan data for unit 28 and upper part of unit 25

Sample interval	Pollen type	Magnification
0-1 cm	Erodium	100X
	Erodium	100X
	Eucalyptus	400X
1-2 cm	Erodium	100X
2-3 cm	Erodium	100X
	Erodium	100X
	Erodium	100X
	Eucalyptus	400X
	Eucalyptus	400X
3-4 cm	Erodium	100X
	Erodium	100X
	Erodium	100X
	Erodium	100X
	Eucalyptus	400X
4-5 cm	Erodium	100X
	Eucalyptus	400X
	Eucalyptus	400X
	Eucalyptus	400X
5-6 cm	Erodium	100X
	Erodium	100X
6-7 cm	none noted	
7-8 cm	Erodium	100X
	Erodium	100X
8-9 cm	Erodium	100X
	Eucalyptus	400X
9-10 cm	Erodium	100X
10-11 cm	Erodium	100X
	Erodium	100X
11-12 cm	Erodium	100X
12-13 cm	none noted	
13-14 cm	none noted	
14-15 cm	none noted	
15-16 cm	none noted	

Microscope magnification at which grain was first noted